IOP Publishing Journal of Physics: Condensed Matter
J. Phys.: Condens. Matter **35** (2023) 455704 (17pp) https://doi.org/10.1088/1361-648X/acee3e

# BEG spin-1 model with random exchange magnetic interactions for spin-crossover solids

**Saliou Bolarinwa Ogou**[1,2], **Toussaint Djidjoho Oke**[1,2,*], **Mounirou Karimou**[1,3], **Félix Hontinfinde**[1] and **Kamel Boukheddaden**[2]

[1] Département de Physique (FAST) et Institut des Mathématiques et de Sciences Physiques (IMSP), Université d'Abomey-Calavi, Abomey Calavi 01 BP 613, Benin
[2] Groupe d'Études de la Matière Condensée (GEMaC), Université Paris-Saclay, Université de Versailles/St. Quentin en Yvelines-CNRS 45 Avenue des Etats Unis, F78035 Versailles Cedex, France
[3] Ecole Nationale Supérieure de Génie Energétique et Procédés (ENSGEP) d'Abomey, Abomey, Benin

E-mail: toussaint.oke@imsp-uac.org

Received 8 June 2023, revised 22 July 2023
Accepted for publication 7 August 2023
Published 21 August 2023

**Abstract**

We have investigated magnetic phase diagrams of spin-crossover (SCO) solids throughout the Blume–Emery–Griffiths spin-1 model where the spin states $\pm 1$ and 0 are associated to high-spin state and low-spin states respectively. In the present work, the quadrupolar interaction, $K$, parameter depends linearly on temperature and accounts for the role of the lattice phonons in the elastic interactions between the SCO units. Magnetic interactions are randomly distributed in the system and are controlled by a factor $\gamma = J_{ij}/K$ such that for $\gamma = 0$ ($J_{ij} = 0$), magnetic ordering is not expected. The crystal-field that acts on SCO sites depends both on the ligand-field strength and the degeneracy ratio between HS and LS states as in some previous works. The system is also under the effect of a random local magnetic field $h_i$ acting on each site $i$. The model is solved using a homogeneous mean field theory. Our investigations reveal the occurrence of thermally-induced gradual, and first-order spin-transitions by varying the model parameters. At vicinity of first-order transition, various types of isothermal magnetic hysteresis loops are obtained and their corresponding coercive field and loop patterns are discussed as function of temperature.

Keywords: spin-crossover solids, BEG model spin-1, mean-field theory, random magnetic field (RMF), random exchange interaction (REI), phase diagrams

(Some figures may appear in colour only in the online journal)

## 1. Introduction

Spin-crossover (SCO) materials with a central metal ion (with 4–7 $d$ electrons) which have the property to switch between two different spin states, have been the object of a large number of studies [1–4]. Their thermodynamic bistability continues to attract enormous interest due to their possible technological applications such as sensors or reversible high-density data storage devices, displays [5–10], molecular switches [5, 11, 12], etc. Moreover, these materials exhibit a variety of thermodynamic behaviors resulting in changes of magnetic, optical and mechanical properties which are the source of rich and dense experimental studies [1–3].

The basic mechanism of the spin transition at the molecular level is encountered in transition metal compounds in octahedral symmetry with 4 to 7 electrons in the 3$d$ orbital, where the ligand field is of the same order of magnitude as the pairing

* Author to whom any correspondence should be addressed.

 

energy between electrons. In this case, the fundamental level is associated to the low-spin (LS) diamagnetic state and the excited one to the high-spin (HS) paramagnetic state. For example, for SCO materials based on iron (II) complexes, which are the most studied ones, the total spin value of the LS state is $\sigma = 0$ and that of the HS is $\sigma = 2$, where $\sigma$ is the true ion total spin. Thus, the influence of various stimuli as external constraints [13–16], induces a population change of both levels. During this phenomenon, named spin-transition [6, 7, 17–20] is mostly occurred on SCO materials which can switch between LS and HS states which affects several of their physical properties [13, 15, 16]. The possible change of spin state allows to obtain devices for high density information storage in which the unit of memory can be reduced to a molecule, thus allowing to reach capacity more important than those of conventional materials. Thermally induced spin transitions lead to both electric and structural changes, often observed as a color and magnetic moment changes [6, 21, 22].

Depending on the type and the strength of the interactions between molecules, SCO compounds present different types of spin-transition. Indeed, when the interactions between molecules is weak, the HS fraction, that is the fraction of molecules occupying the HS state, displays a continuous and gradual, changes with temperature, whereas in the case of a strong intermolecular coupling, the SCO solids system exhibit cooperative phenomena [23–25], which manifest through the existence of first-order phase transitions accompanied with thermal hysteresis, whose widths directly relate to the strength of the interactions in the lattice. In addition, it has been shown in several works [23, 24, 26], that the elastic interactions are at the hearth of the existence of cooperative effects in SCO materials. Experimental results also reveal that SCO transitions involve both electronic transformation (spin and orbital) and structural modifications [2, 6, 26–29].

Theoretically, several models have been considered to describe the thermodynamic behaviors of SCO materials. Most of them are based on Ising-like models [30–32], atom–phonon coupling [17, 22, 33–36], elastic descriptions [37, 38] or other complex elastic approaches [23, 29, 39–42] taking into account the volume change at the transition. These models are solved analytically using mean-field approaches or by Monte Carlo (MC) simulations [17, 23, 39] or using molecular dynamics [24, 43] techniques. Recently, a Blume–Emery–Griffiths (BEG) model with spin-phonon interactions has been adapted to study SCO materials. This model has been solved using corrective effective-field theory (CEFT) and kinetic MC simulations with Glauber dynamics [44] or dynamic mean-field theory (DMFT) approach [45–47] or the Bethe lattice (BL) approach and MC simulations with Arrhenius dynamic [48, 49]. In these works, the quadrupolar coupling parameter $K$ is assumed to depend linearly on the absolute temperature $T$ in the form $K = \alpha k_B T$, which mimics the role of the phonon lattice in the interactions between the SCO units. The effective energy gap $D$ between the LS and the HS states depends on the absolute temperature $T$, the degeneracy ratio $g$ between LS and HS states and the 0 K ligand-field strength $\Delta$.

In the past, several methods were used to solve spin-1 Ising-like model with random bonds [50] or the spin-$\frac{3}{2}$ Ising model with both random crystal-field and random biquadratic exchange interactions [51] or mixed spins models with random crystal field (or random bonds) [52–54] which exhibited interesting physical properties.

Generally, by addressing SCO and Prussian blue analogs (PBAs) materials, the spin-transition phenomena are reliable to the microscopic configuration leading to the interactions nature between central metallic atoms located to the lattice sites' [1–14]. In regular crystal lattice, the intermolecular elastic interactions originating from misfit between the molecular volumes in different spin states generate very rich behaviors. Because of the different energies and degeneracies between the fundamental states HS and LS, the microscopic Ising-like model [17, 22–24, 26–28, 30–36, 39–43] describes very well the behavior of these SCO systems. In this case, the intermolecular interaction is considered in the fully connected limit with the following BEG-like model Hamiltonian [44–49]:

$$H = -J\sum_{<i,j>}\sigma_i\sigma_j - K\sum_{<i,j>}\sigma_i^2\sigma_j^2 + D\sum_i\sigma_i^2 - h\sum_i\sigma_i, \quad (1)$$

where $\sigma_i$ is the fictitious classical spin (pseudospin) for each site $i$ ($i = 1, 2, \ldots, N$ and $N$ the total number of sites). In each site $i$, the spin can have $\sigma_i = \pm 1$ (0) as eigenvalues in HS (LS) states. The first term in the model (1) describes the intermolecular interactions of elastic origin through a phenomenological parameter expressed as $\gamma = J/K$ from which $J$ ($>0$ in ferromagnetic-like systems) also depends linearly with the temperature and accounts for coupling nearest-neighbors ($nn$) sites $i$ and $j$. The second and the third terms account for the quadrupolar and crystal-field contributions with the total energy in the case of isotropic lattice structure, which are previously described with the parameter $K$ and $D$. The effective crystal-field $D = \Delta - k_B T \ln g$ is entropic term which is originated from the disorder between the fundamental electronic states (HS and LS states) and the vibronic factor. Due to the both degree of freedom (electronic and vibronic), $g = g_{HS}/g_{LS}$ is relative degeneracy of SCO states where the degeneracy of an HS excited state $g_{HS}$ is necessarily larger than degeneracy of an LS ground one $g_{LS}$. The last sum take account for the Zeeman effect [33, 42] as external magnetic-field $h$ acting in each site $i$ of the spin lattice configuration. Then, each site $i$ feels the corresponding magnetic-field applied magnetic-field [55, 56]. Usually, $g$ (known as Landè factor) depends on temperature through the temperature dependence of the phonon density of the lattice [33, 56]. In real systems of SCO and PBAs, due to the impurities inside the anisotropic crystal, the interactions through the systems can be modeled randomly to take account the vacancies sites [57, 58]. Theoretically, from the point of view of Ising model, the local random magnetic-field comes from impurities, generates random interactions and that reflect a local quenched and bond length between atomic sites. A novel feature of SCO systems consists in the fact that substitutional disorder generates local quenched and random bond length which are circumstance plays an important role during the spin-transition. Such that, we consider the exchange magnetic interactions as $J_{ij}$ (taken as constant

between *nn* spins usually describe in Ising-like models), that are the infinite-range quenched random elastic interactions between the pseudospin degrees of freedom which represent the magnetic states of central transition metal ions within the ligands. For these systems, every site is in a specific local environment, generated by a ligand with particular features, and rather are not equivalent to each other. Then, the impurities are considered as many vacancies/disorder of lattice sites that are introduced randomly in local elastic forces and in external magnetic-field (noted here as $h_i$) created between SCO molecules in different magnetic states. This justifies well such a study carried out on SCO systems in the case of random exchange interactions (REIs) between the atomic sites and the random magnetic field (RMF) which acting in each of these sites.

In the present investigation, as described previously, we consider the BEG-type model for SCO solids with REIs and RMF that we solve within the mean field theory (MFT). Despite this method neglects nonlocal fluctuations, thermal multi-transition is obtained through intermediate magnetic states as stable, metastable and unstable, for that with MC simulations, only stable states can be obtained. The derived mean-field equations are numerically solved for the magnetization $m$ and the HS fraction, $n_{\rm HS}$, of molecules in the HS state. Thermal phase diagrams are derived from the thermal variations of these order-parameters. In addition, magnetic hysteresis takes place when the system is submitted to an external magnetic field. The coercive fields are reported as function of the temperature for selected values of other model parameters.

The remainder of this paper is organized as follows. The next section 2 is devoted to the presentation of the model and the description of the used calculation method. In section 3, we present and discuss the obtained numerical results. In section 4 we conclude and outline some possible extensions of this work.

## 2. The model Hamiltonian and mean-field equations

The Hamiltonian of the spin-1 BEG model with REI and RMF is written as follows:

$$H = -\sum_{<i,j>} J_{ij}\sigma_i\sigma_j - K\sum_{<i,j>}\sigma_i^2\sigma_j^2 + D\sum_i \sigma_i^2 - \sum_i h_i\sigma_i, \quad (2)$$

where $\sigma_i = \pm 1, 0$ are fictitious spin values located at site $i$ of a square lattice. The spins $\sigma_i = \pm 1$ describe the magnetic HS spin state and $\sigma_i = 0$ is associated to the diamagnetic LS state. Here, we consider only the *nn* interactions for the pairing $< i,j >$. In equation (2), $J_{ij}$ denotes the ferromagnetic REI parameter between the magnetic states ($\sigma_i = \pm 1$); $K$ is the quadrupolar interaction between neighboring SCO sites. Due to the elastic nature of the SCO transition [39–43], this $K$ term that takes into account the phonon contribution is written here as $K = \alpha k_{\rm B}T$ [44, 45, 48, 49, 55] with the ratio $\gamma = J_{ij}/K$ taken as an adjustable parameter. The effective ligand-field strength $D$ which originates from the entropy term, is assumed to depend on the absolute temperature $T$ of the system, the degeneracy ratio $g$ between LS and HS states and the ligand-field energy splitting $\Delta$. It is written as $D = \Delta - k_{\rm B}T\ln(g)$ (see [44, 48, 49, 55]). Finally, $h_i$ is the RMF acting on the lattice SCO site $i$.

In order to write the mean field equations, let us denote by $H_i$, the one-site Hamiltonian that each site $i$ feels throughout the spins lattice. In the MFT approach, $H_i$ reads [48]:

$$H_i = -m\sigma_i\sum_j J_{ij} - zKn_{\rm HS}\sigma_i^2 + D\sigma_i^2 - h_i\sigma_i, \quad (3)$$

where $m = \langle\sigma_i\rangle$ and $n_{\rm HS} = \langle\sigma_i^2\rangle$ are considered as invariant by translation over the lattice. The associated mean field free energy function per site is given by

$$f(J_{ij},h_i) = U(J_{ij},h_i) - TS(J_{ij},h_i), \quad (4)$$

where $U(J_{ij},h_i)$ and $S(J_{ij},h_i)$ are the internal energy and entropy per site of the system, respectively given by:

$$U(J_{ij},h_i) = -\frac{m^2}{2}\sum_j J_{ij} - \frac{z}{2}Kn_{\rm HS}{}^2 + Dn_{\rm HS} - h_i m, \quad (5)$$

$$S(J_{ij},h_i) = k_{\rm B}\beta < H_i > + k_{\rm B}\ln\sum_\sigma \mathrm{e}^{-\beta H_i}. \quad (6)$$

$\beta = \frac{1}{k_{\rm B}T}$ and $\langle H_i\rangle = -m^2\sum_j J_{ij} - zKn_{\rm HS}{}^2 + Dn_{\rm HS} - h_i m$ is the average value of $H_i$, where $z$ is lattice coordination number. After some calculations, one gets the following expression of the net free energy:

$$f(J_{ij},h_i) = \frac{m^2}{2}\sum_j J_{ij} + \frac{z}{2}Kn_{\rm HS}{}^2 - k_{\rm B}T\ln\left[1 + 2\mathrm{e}^{\beta(zKn_{\rm HS}-D)}\cosh\beta(zJ_{ij}m + h_i)\right]. \quad (7)$$

Both REI and RMF that act on the system are respectively distributed according to the probability laws:

$$\begin{cases} P(J_{ij}) = q\delta(J_{ij} - J) + (1-q)\delta(J_{ij} - \lambda J) \\ P(h_i) = p\delta(h_i - h) + (1-p)\delta(h_i - \lambda h). \end{cases} \quad (8)$$

Here, it is important to mention that we take, for simplicity, a bimodal distribution of exchange interactions and magnetic-field distributed randomly belong the spin-lattice configurations. In real situation, to take account a disorder coming from the system impurities, the local fields generated are randomly distributed and affected the local elastic forces between SCO molecules in different magnetic states. This lead to a 'random interactions' and 'random local magnetic-field' that are in the heart of the disorder introduced in the new version of this Ising-like model. The random interactions $J_{ij}$ (random local magnetic-fields $h_i$) are independently distributed according to Gaussian probability $P(J_{ij}) \sim \exp\left[-(J_{ij}-J)^2/2\sigma^2\right]$ ($P(h_i) \sim \exp\left[-(h_i-h)^2/2\sigma^2\right]$) [57, 58] where the symbol $\sigma$ refers to the standard deviation as fluctuations on each parameter considered in the distribution.

Above, in these two last equations, $q$ and $p$ are probability of having $J$ exchange interaction and $h$ magnetic field. Thus, the first terms in equation (8) impose that, in the total

lattice, an amount of $z \times q\frac{N}{2}$ *nn* bonds ($p \times N$ spins) are under the influence of exchange interaction $J$ (magnetic field $h$). As for the second term, the parameter $\lambda$ is introduced so that the strength of exchange interaction $J$ (magnetic field $h$) is altered on an amount of $z(1-q)\frac{N}{2}$ *nn* bonds ($(1-p)N$ spins) remaining with respect to the first one. So, the parameter $\lambda$ is taken such as $0 \leqslant \lambda \leqslant 1$. In the range of our system parameters values, these distribution lead to some well-known models: (i) the BEG model when $p=1$ and $q=1$ or $0 \leqslant p < 1$, $0 \leqslant q < 1$ and $\lambda = 1$; (ii) the bond-diluted model when $0 \leqslant q < 1$, $h=0$ and $\lambda = 0$ [50]; (iii) the random bond BEG model for $p=1$, $0 < q < 1$ and $0 \leqslant \lambda < 1$ and (iv) the RMF BEG model if $q$ is set to 1 with $0 < p < 1$ and $0 \leqslant \lambda < 1$.

Now, we can integrate equation (7) over the $P(J_{ij})$ and $P(h_i)$ to get the variational free energy of the system. Thus, the integration below has to be carried out as:

$$F(m, n_{\mathrm{HS}}, T) = \int P(h_i)\mathrm{d}h_i \int f(J_{ij}, h_i) P(J_{ij})\mathrm{d}J_{ij}. \tag{9}$$

After some simple calculations, the variational free energy of system is given by

$$\begin{aligned} &F(m, n_{\mathrm{HS}}, T) \\ &= \frac{z}{2}qJm^2 - \frac{z}{2}q\lambda Jm^2 + \frac{z}{2}\lambda Jm^2 + \frac{z}{2}Kn_{\mathrm{HS}}^2 \\ &\quad - qpk_{\mathrm{B}}T\ln[1 + 2\mathrm{e}^{\beta(zKn_{\mathrm{HS}}-D)}\cosh\beta(zJm+h)] \\ &\quad - q(1-p)k_{\mathrm{B}}T\ln[1 + 2\mathrm{e}^{\beta(zKn_{\mathrm{HS}}-D)}\cosh\beta(zJm+\lambda h)] \\ &\quad - (1-q)pk_{\mathrm{B}}T\ln[1 + 2\mathrm{e}^{\beta(zKn_{\mathrm{HS}}-D)}\cosh\beta(z\lambda Jm+h)] \\ &\quad - (1-q)(1-p)k_{\mathrm{B}}T\ln[1 + 2\mathrm{e}^{\beta(zKn_{\mathrm{HS}}-D)}\cosh\beta(z\lambda Jm+\lambda h)]. \end{aligned} \tag{10}$$

Then, we present here the order parameters which are obtained by minimizing the free energy function followed by the integration over the $P(J_{ij})$ and $P(h_i)$ as we did previously. Thus, the magnetization $m$ and the $n_{\mathrm{HS}}$ fraction are given by the following system equations:

$$\begin{cases} \frac{\partial F(m,n_{\mathrm{HS}},T)}{\partial m} = 0, \\ \frac{\partial F(m,n_{\mathrm{HS}},T)}{\partial n_{\mathrm{HS}}} = 0. \end{cases} \tag{11}$$

After some calculations, one gets the following self-consistent equation:

$$\begin{aligned} m = {} & qp\frac{2\sinh\beta(zJm+h)}{\mathrm{e}^{-\beta(zKn_{\mathrm{HS}}-D)} + 2\cosh\beta(zJm+h)} \\ & + q(1-p)\frac{2\sinh\beta(zJm+\lambda h)}{\mathrm{e}^{-\beta(zKn_{\mathrm{HS}}-D)} + 2\cosh\beta(zJm+\lambda h)} \\ & + (1-q)p\frac{2\sinh\beta(z\lambda Jm+h)}{\mathrm{e}^{-\beta(zKn_{\mathrm{HS}}-D)} + 2\cosh\beta(z\lambda Jm+h)} \\ & + (1-q)(1-p)\frac{2\sinh\beta(z\lambda Jm+\lambda h)}{\mathrm{e}^{-\beta(zKn_{\mathrm{HS}}-D)} + 2\cosh\beta(z\lambda Jm+\lambda h)}, \end{aligned} \tag{12}$$

$$\begin{aligned} n_{\mathrm{HS}} = {} & qp\frac{2\cosh\beta(zJm+h)}{\mathrm{e}^{-\beta(zKn_{\mathrm{HS}}-D)} + 2\cosh\beta(zJm+h)} \\ & + q(1-p)\frac{2\cosh\beta(zJm+\lambda h)}{\mathrm{e}^{-\beta(zKn_{\mathrm{HS}}-D)} + 2\cosh\beta(zJm+\lambda h)} \\ & + (1-q)p\frac{2\cosh\beta(z\lambda Jm+h)}{\mathrm{e}^{-\beta(zKn_{\mathrm{HS}}-D)} + 2\cosh\beta(z\lambda Jm+h)} \\ & + (1-q)(1-p)\frac{2\cosh\beta(z\lambda Jm+\lambda h)}{\mathrm{e}^{-\beta(zKn_{\mathrm{HS}}-D)} + 2\cosh\beta(z\lambda Jm+\lambda h)}. \end{aligned} \tag{13}$$

We can also estimate the thermal average value deviation of magnetization which well-known as magnetic susceptibility given by the formula,

$$\chi = \frac{1}{k_{\mathrm{B}}T}\left(n_{\mathrm{HS}} - m^2\right). \tag{14}$$

In order not to overload the figures, the behavior of the magnetic susceptibility $\chi$ is not represented, but its character values are found through the phase diagrams.

After having obtained the self-consistent expressions (12) and (13), where the order parameters $m$ and $n_{\mathrm{HS}}$ are coupled, we solve them numerically using Newton–Raphson method, to study their thermal behaviors and to derive the phase diagrams of the system in the ($\gamma$, $T_{\mathrm{C}}$) and ($h$, $T_{\mathrm{C}}$) planes for given values of $q$, $p$, and $\lambda$. This is done in the next section. Note that in this work, the coordination number $z$ is taken equal to 4 due to the square symmetry of the system.

## 3. Results and discussions

From the point of view of equilibrium properties, thermodynamic quantities are presented in this section for a ferromagnetic SCO system under RMF and REI which act on each site and bond, respectively, within the configuration spin lattice. In the spin-transition region, selected values of model parameters' are used to reproduce significant results. Then, the ligand-field energy is set to the value of $\Delta = 400\,\mathrm{K}$ and the degeneracy ratio value between LS and HS spin states is presented by $g = 100$. This value of parameter $g$ leads to a molar entropy change at the transition $\Delta S = R\ln(g) \simeq 38.29\,\mathrm{J{\cdot}mol^{-1}\cdot K^{-1}}$ which is in agreement with the experimental data in literature [39, 59] where $\Delta S$ values are in the range of 35–80 $\mathrm{J\cdot mol^{-1}\cdot K^{-1}}$. The chosen ligand-field energy $\Delta$ value leads to a molar enthalpy variation at the transition $\Delta H \propto N_{\mathrm{A}}\Delta \simeq 3.324\,\mathrm{kJ\cdot mol^{-1}}$ where $N_{\mathrm{A}}$ is Avogadro number. This enthalpy change consists of the zero-point energy difference [57, 58], the electronic energy change between HS and LS states and the vibrational energy difference. The increase in the value of $\Delta$ leads to an increase in the value of $\Delta H$ as well as the transition temperature $T_{\mathrm{c}}$. Molecular deposition on substrate case leads to zero-point energy correction that enhanced the enthalpy change involving on the SCO phenomena [60]. The external magnetic field $h$ is in the range of $[-350; +350]\,\mathrm{K}$ in pure Ising-like SCO system. This range of values of the magnetic-field helps us to reproduce significant spin states in our model

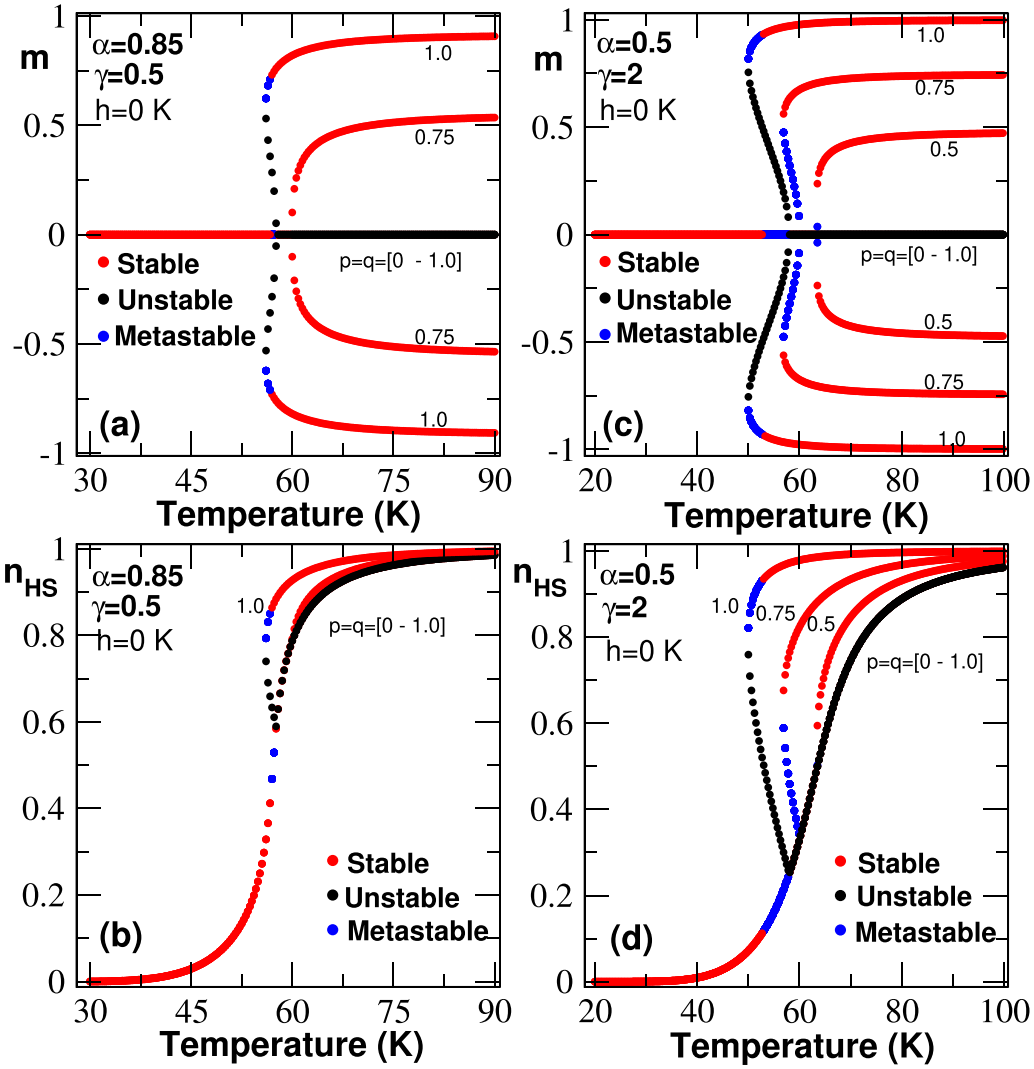


**Figure 1.** Thermal behaviors of the order parameters (magnetization $m$ and $n_{\mathrm{HS}}$ fraction) in absence of magnetic field for selected values of $p(=q)$. In panels (a) and (b) : $\alpha = 0.85$ and $\gamma = 0.5$; while in panels (c) and (d), $\alpha = 0.5$ and $\gamma = 2$. The curves shift slightly to the low-temperature region for increasing values of $p$ and $(q)$ with an enhancement of their steep character, accompanied with the appearance of a thermal hysteresis. In panels (a) and (c), symmetric solutions (multiple states) are obtained with respect to $m = 0$ in the magnetization $m$ behaviors that saturated its values at $\pm p(q)$ while $n_{\mathrm{HS}}$ is saturated at 1 (panels (b) and (d) at high temperature.

Hamiltonian during the spin-transition in its entirety throughout the phase diagrams. First, we analyze the physical properties of the system at thermal equilibrium in relation with $p, q$ and $\lambda$ values.

### *3.1. Thermal dependence of HS fraction and magnetization*

We first present results on the thermal behaviors of the order parameters, which are useful in obtaining thermal phase diagrams of the system. For that, $p$ and $q$ are set to the same value for simplicity and varying in [0–1] range of probability values in equations (12) and (13). These mean that one part of lattice sites (bonds) are under the influence of magnetic field $h$ (exchange interactions $J$) and the rest submitted to $\lambda h$ ($\lambda J$). This allows to consider a kind of partition of the magnetic sublattice following a certain distribution of defects both on sites and bonds with probabilities $p$ and $q$ respectively. Different values of $p$ and $q$ used in the description of the system lead globally to the same conclusion according to the effects of the parameters on the model Hamiltonian. In addition, the effect of $\lambda$ on the SCO sub-lattice is studied through the analysis of the thermal dependence of the HS fraction for $\lambda$ values taken in the interval [0–1].

To facilitate the comprehension of this study, we first begin by examining the behavior of the system in zero field ($h = 0$) and $\lambda = 0$, the results of which are brought together in figure 1. In this figure, are represented the thermal behavior of magnetization $m$ and fraction HS, $n_{\mathrm{HS}}$, for selected magnetic exchange and elastic coupling values. It is revealed that according to the permissible solutions of the self-consistent equations (12) and (13), stable, metastable and unstable states appear depending on the couple of values ($\alpha$, $\gamma$) enabling to switch from a second-order to a hysteretic first-order transition with transition temperature values, 56–62 K and 49–64 K, respectively in panels (a), (b) and (c), (d) when for increasing values of the couple $(p, q)$. Furthermore, panels (a) and (c) showing

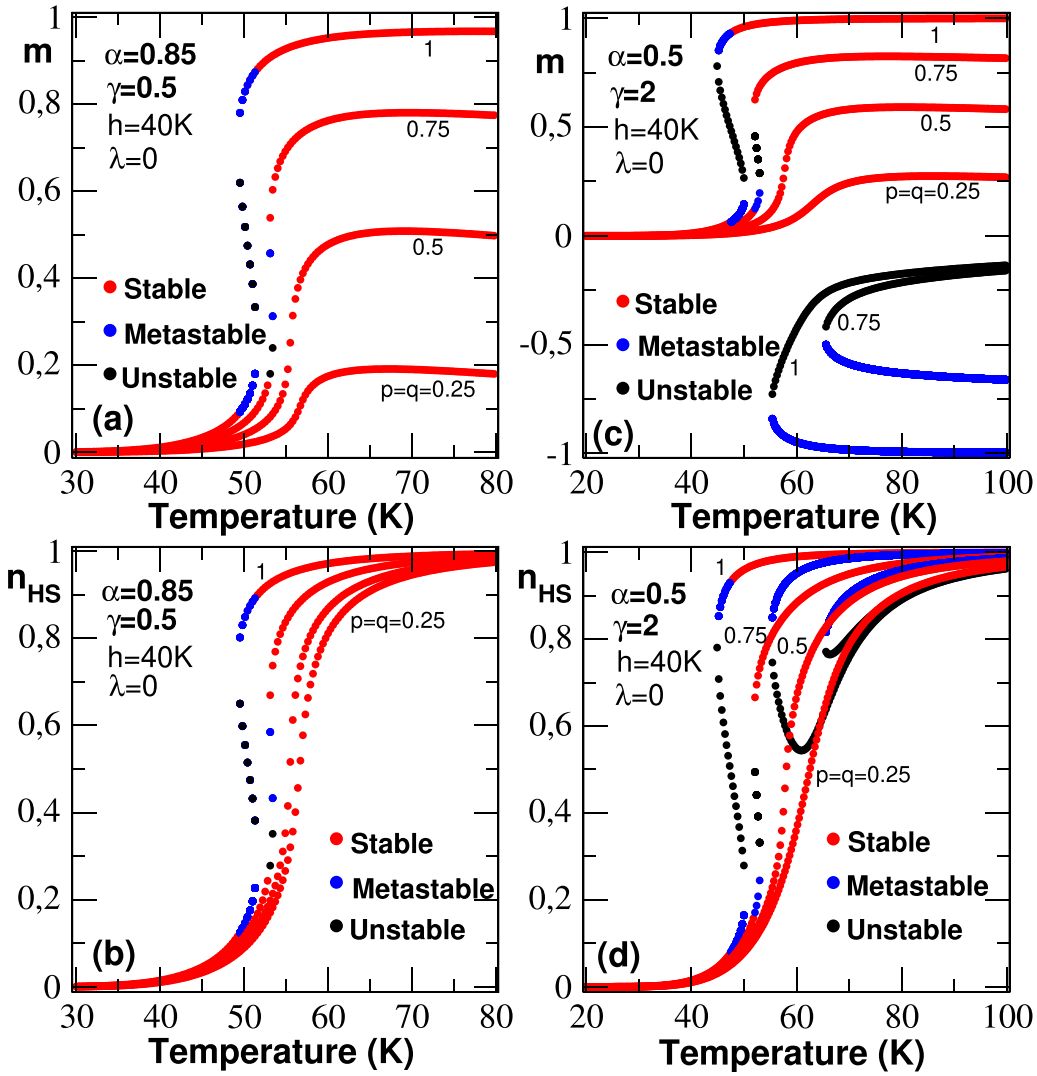


**Figure 2.** Thermal behaviors of the order parameters (magnetization $m$ and $n_{\rm HS}$ fraction) for selected values of $p(=q)$. In panels (a) and (b): $\alpha = 0.85$ and $\gamma = 0.5$; while in panels (c) and (d), $\alpha = 0.5$ and $\gamma = 2$. The curves shift to the low-temperature region for increasing values of $p$ and $(q)$ with an enhancement of their steep character, accompanied with the appearance of a thermal hysteresis. For low value of $p$ and $(q)$, incomplete spin-transition occurs while $m$ and $n_{\rm HS}$ are saturated their values to $\pm 1$ and 1, respectively for $p(=q) = 1$.

the thermal behaviour of the magnetization, clearly display symmetric solutions with respect to $m = 0$ (trivial solution in equation (12) for $h = 0$) converting from the diamagnetic state (at low-temperature) to a ferromagnetic state at high temperature. At the transition temperatures, the different phases overlap, so that it cannot distinguish them according to the color codes of the states indicated for different values of $p(q)$. For $p(q) = 0.75$ of panel (a), $m = 0$ is a stable solution at low temperatures but it becomes unstable for all temperatures above the critical temperature. When $p(q)$ are increased to 1, $m = 0$ is both stable, metastable and unstable around the critical temperature, it becomes stable and unstable below and above this critical temperature, respectively. Similar trends are obtained in panel (c) of this figure when $p(q)$ value is between 0 and 1. We notice that at high temperatures, $m = 0$ can have different meaning and at high temperatures, stable, metastable and unstable phases prevail with non-zero magnetization as depicted in figure 4. Obviously, Ising-like model leads to the transition temperature as $k_{\rm B}T_{\rm c} = Jz$ for which in the present model, $J$ is temperature-dependent (as $J_{ij} \sim T$), that leads to none-zero magnetization for $h \neq 0$ at high temperatures. Moreover, it remains a stable one below/above the critical temperature when $\gamma = 0$ (for none magnetic interactions) for $p(q) = 1$ which corresponds to the situation of figure 1(a) of [46]. As stated above, the first-order character of these transition curves vanishes below some threshold $p$ and $q$ values, for which the magnetization reaches the values $\pm p$ at saturation. However, this first-order character predominates on increasing $\gamma$ value. The corresponding HS fraction dependencies, gathered in panels (b) and (d), shows that $n_{\rm HS}$ presents the same trends, since for $p = q = 0.75$ a gradual continuous transition is obtained, which converts to first order for higher $p$ and $q$ values. The first-order character of the transition is also strengthened on increasing the elastic interaction, $\gamma$. It is remarked here, that contrary to $m$, the HS fraction saturates at 1 in the high temperature regime whatever $p$ and $q$ values, due

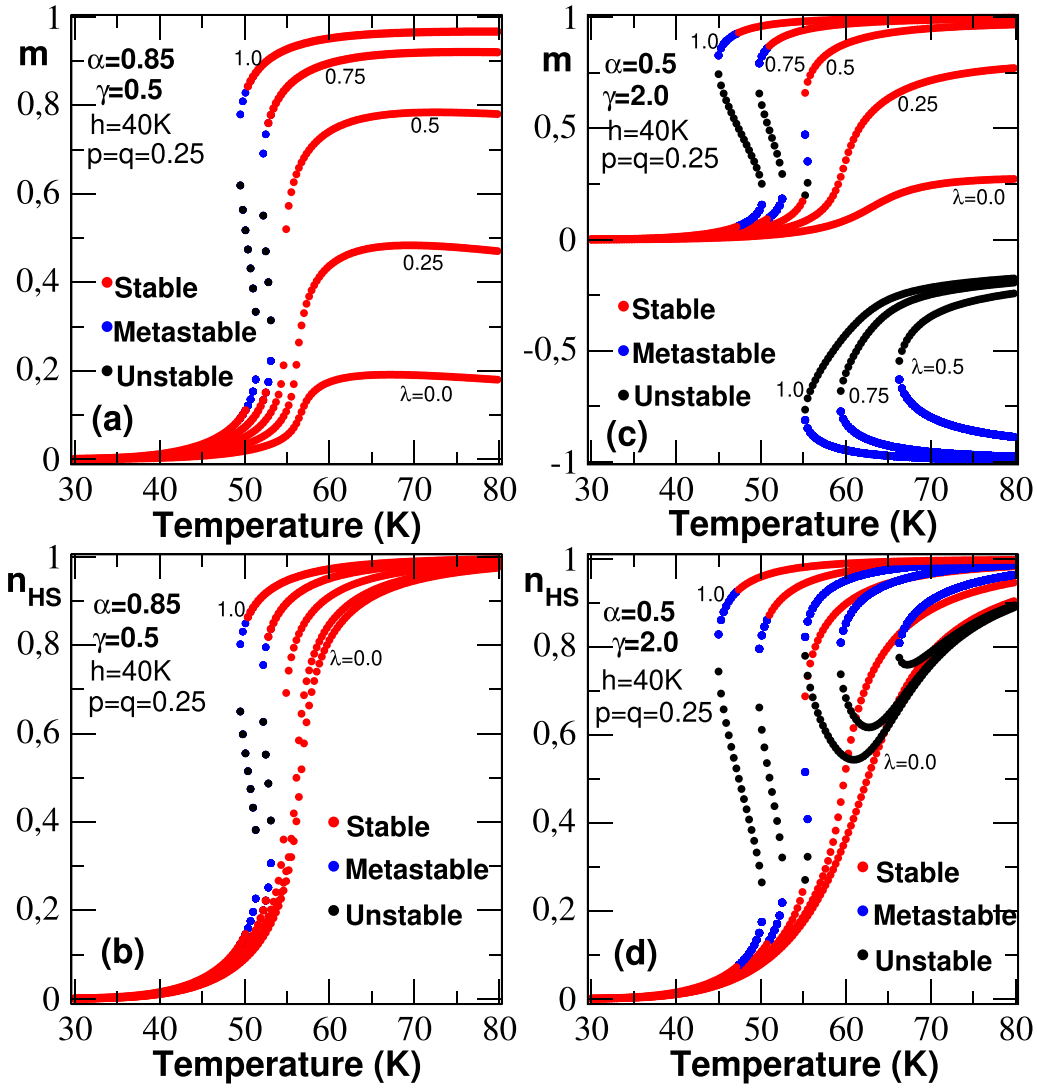


**Figure 3.** Thermal behaviors of the order parameters (magnetization $m$ and $n_{HS}$ fraction) for selected values of $\lambda$ and at fixed value of $p = q = 0.25$. (a), (b) $\alpha = 0.85$ and $\gamma = 0.5$; (c), (d) $\alpha = 0.5$ and $\gamma = 2$. The curves shift to the low-temperature region for increasing values of $\lambda$ as in figure 2. For low value of $\lambda$, incomplete spin-transition occurs while $m$ and $n_{HS}$ tend to their saturated values when $\lambda$ value increases up to 1.

to the fact that we restricted here the effect of the dilution to the magnetic subsystem.

When an external magnetic field is applied to the system, the number of solutions decreases as $p(q)$ increases with a topological difference of the solutions whose analyses are carried out in the following figures.

Figure 2 illustrates the temperature-dependence of the magnetization $m$ (panels (a) and (c)) and HS fraction $n_{HS}$ (panels (b) and (d)) for varying values of $p$ and $q$ at fixed values for the reduced interaction parameters, $\alpha$ and $\gamma$. This figure is realized under the condition $\lambda = 0$. This means that the local magnetic exchange (resp. field) interaction $J_{ij}$ (resp. $h_i$) is randomly distributed between the values $J$ (resp. $h$) and 0. As a first remark, the curves of the magnetization, $m$, lose their symmetric character, observed in figure 1, due to the symmetry breaking induced by the nonzero magnetic field.

It clearly appears from figure 2 that starting from the ordered magnetic lattice for $p = q = 1$, showing a first-order transition between a ferromagnetic and diamagnetic phases, and lowering $p$ and $q$ values leads to incomplete and gradual magnetic transitions, with a refocusing of the magnetic transition temperature upon higher values, as depicted in panels (a) and (c), obtained for both tested parameter values of $\alpha$ and $\gamma$ corresponding to the quadrupolar ($K$) and the magnetic ($J$) interactions, respectively. Thus, the value of the net magnetization at saturation in the high temperature phase, drops from the value 1 for $p = q = 1$ to $\sim 0.2$ for $p = q = 0.25$, where a very partial ferromagnetic order is obtained in the high-temperature limit. Concomitantly, panels (b) shows that the HS fraction transforms for the usual hysteretic first-order transition for $p = q = 1$ to a gradual one when $p$ and $q$ values are decreased. However, even for $p = q = 0.25$, $n_{HS}$ always

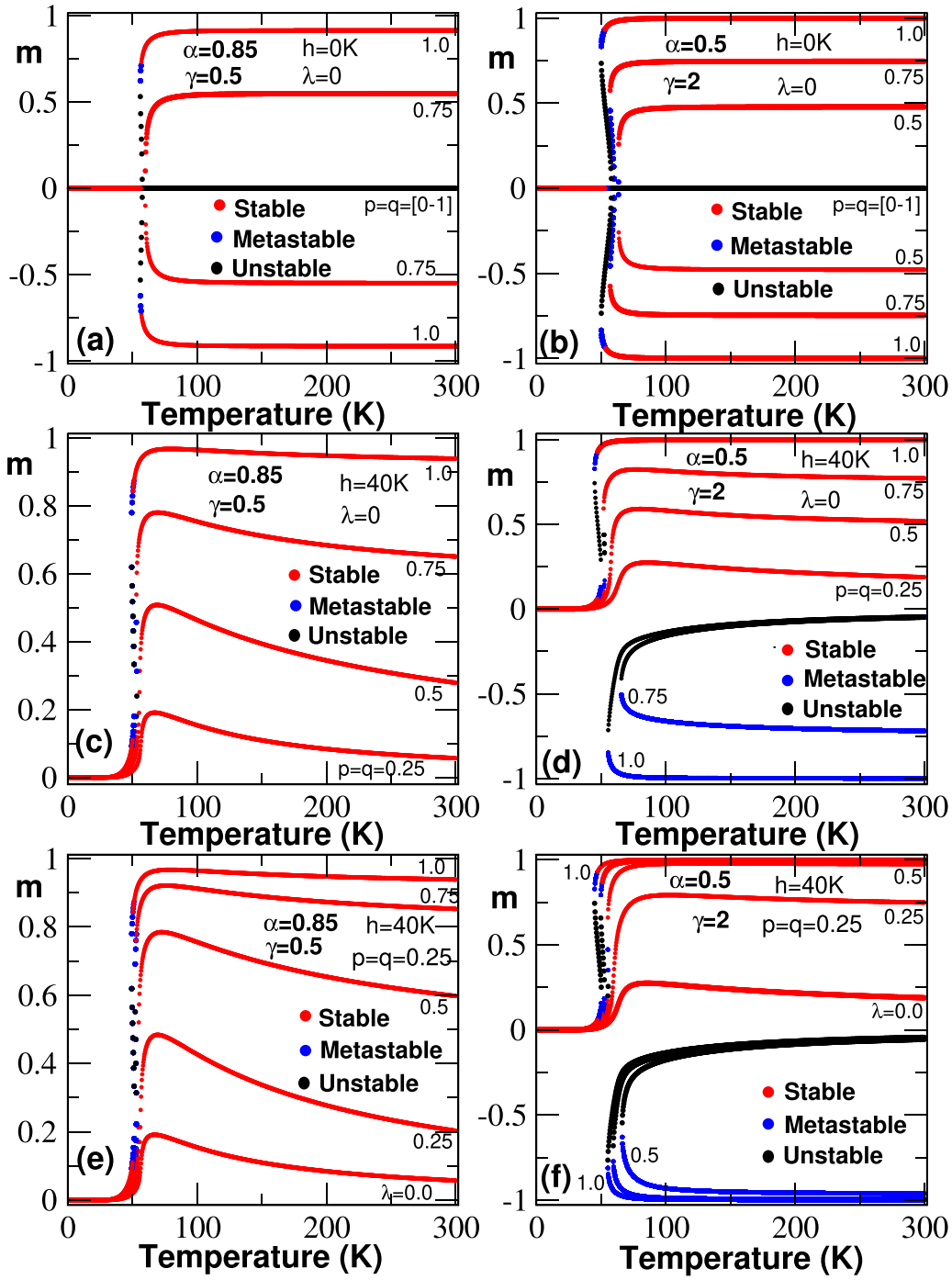


**Figure 4.** Thermal behaviors of the magnetization $m$ at high temperature obtained from panels (a) and (c) of figures 1–3. Same model parameters are used.

reaches the complete HS state ($n_{\rm HS} = 1$), although the transition temperature of the SCO system is also shifted to higher values on decreasing $p$ and $q$ values.

On the contrary, for $p$ ($q$) $\geqslant 0.75$, one observes jumps in the behaviors of the order parameters while their saturate values are quite different from panel (a) to panel (c) for $m$ (panel (b) to panel (d) for $n_{\rm HS}$). As in our previous works, one assists to a high contribution of spin–phonon interactions and lattice elastic constants which often induce first-order transitions [44, 45, 48, 49] for increasing $\alpha$ or $\gamma$ values. Here, as we already stated above, this first-order transition becomes sharper and sharper with increasing the probabilities $p$ and $q$ values. At the same time, the magnetization $|m|$ also increases and tends to the maximum value $+1$ at high temperature, in the HS phase. Obviously, this is due to the non-zero exchange interaction, $J_{ij} = \gamma K = \gamma\alpha \times k_{\rm B}T$ which also increases with temperature, thus favoring the creation of HS units which strongly interact magnetically in the system. Indeed, for $\alpha = 0$, the exchange magnetic coupling is zero ($J_{ij} = 0$), and a paramagnetic phase polarized with the field $h$ appears as soon as

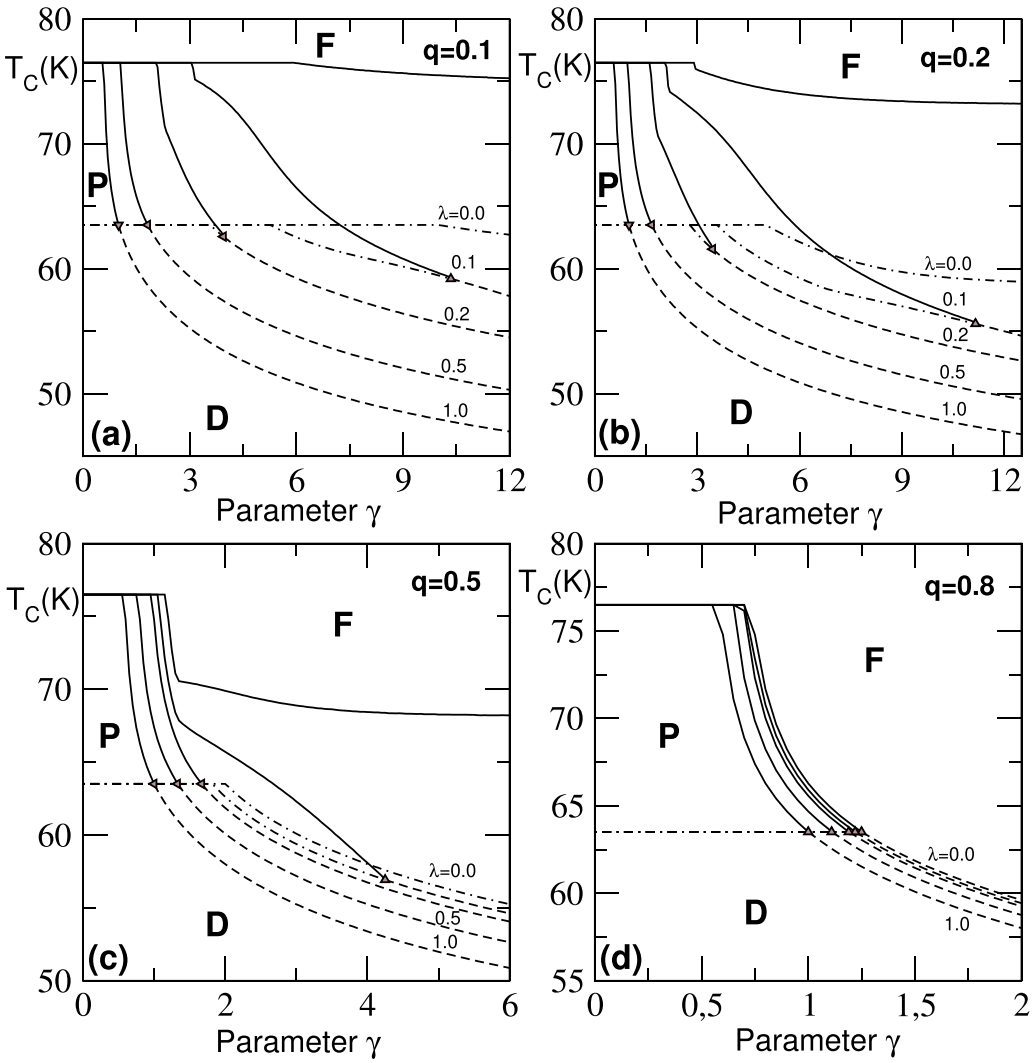


**Figure 5.** Thermal phase diagrams of the model in the ($\gamma$, $T_C$) plane for selected values of the probability $q$ and varying values of the parameter $\lambda$ in the absence of magnetic field. Three phases are found: dia- (D), para- (P) and ferro- (F) magnetic phases. The triangles denote positions of TCP at critical values $\gamma^{TCP}$. For $\lambda = 0$, the TCP does not exist when $q \leqslant 0.5$ (see panels (a)–(c)). Full-lines correspond to positions of critical temperatures $T_C$, dashed-lines are associated to positions of first-order transition temperatures $T_{fo}$ and dashed–dotted lines denote positions of the equilibrium temperature $T_{eq}$. Other values of parameters are: $p = 1$ and $\alpha = 0.5$.

a fraction of HS phase emerges in the system. If one considers the case $p = q = 1$ of figure 2, for example, we see that a sharp SCO transition occurs at $T \simeq 50$ K, at which the sharp, in the case of $p = q = 1$, for the elastic interaction parameter, $K = 42.5$ K in panels (a), (b) and $K = 25$ K in panels (c), (d), while the exchange magnetic coupling may have the values $J = K/2$ and $J = 2 \times K$, respectively. This behavior clearly validates the expected immediate effect of the random exchange magnetic interaction on the SCO transition when the temperature increases. As already shown in our previous works, the stable, metastable and unstable states are obtained according to the competition of the interactions in the model. The magnetic field $h > 0$ ($\lambda > 0$) tends to align the majority of the spins in its direction and few metastable or unstable solutions($m < 0$) are obtained according to its value (for weak magnetic field), leading to $m = -1$ and $n_{HS} = 1$ at high temperature as shown in panels (c) and (d) of figure 2. Moreover, we have also examined, in figure 3, the case of varying $\lambda$ values for fixed $p = q = 0.25$. The thermal dependencies of the $n_{HS}$ and $m$ show a great similarity with those obtained in figure 2.

One can conclude that the spin transition occurs either by a gradual spin conversion to HS state or through a first-order transition according to used values of model parameters. This means that intermediate spin states can be created with gradual spin conversion or first-order transition through the proportion of the presence of impurities/vacancies sites controlled by the probabilities $p(q)$ and the parameter $\lambda$.

*3.1.1. Phase diagrams.* Figures 5–8 collect the phase diagrams of the system. Using temperature corresponding to the maximum of the response function, finite temperature

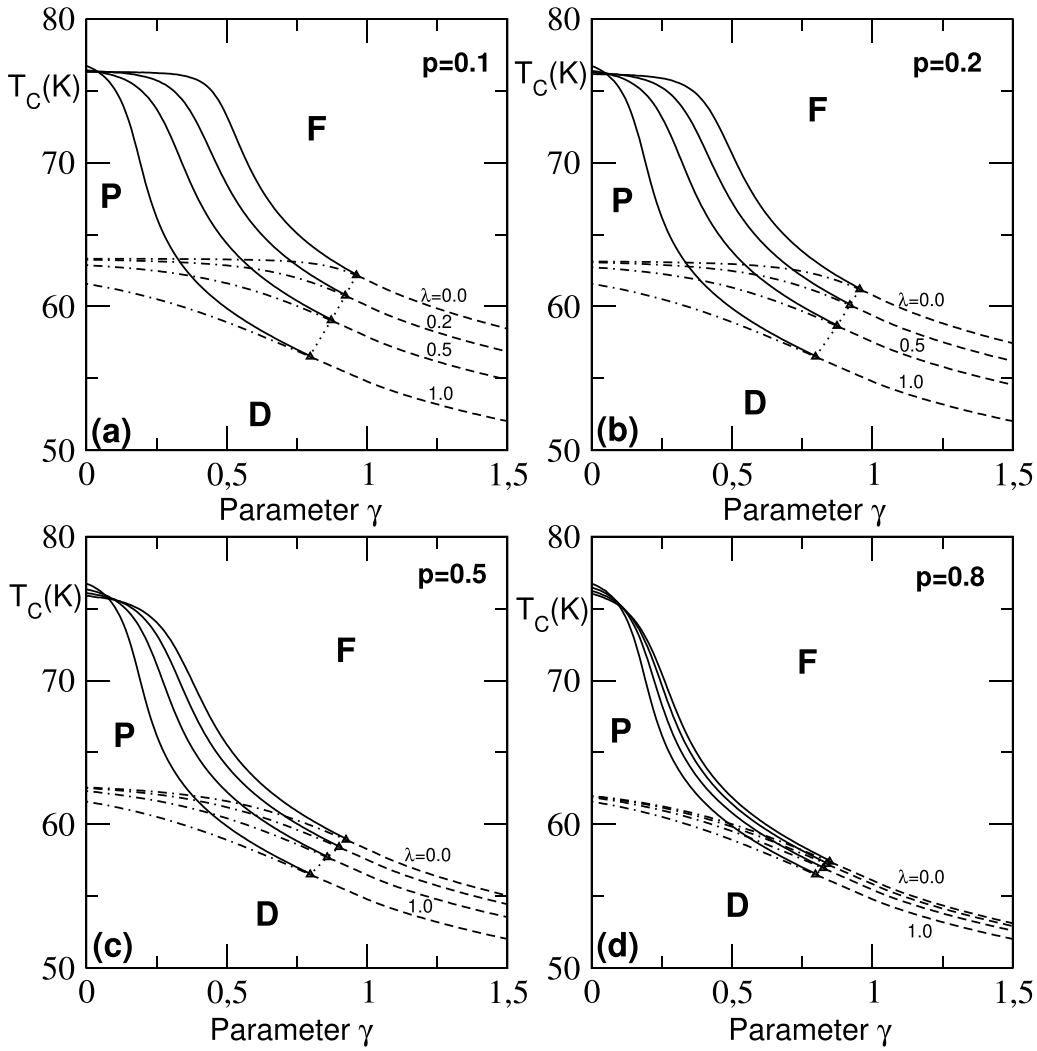


**Figure 6.** Thermal phase diagrams of the system in ($\gamma$, $T_C$) plane for selected values of the probability $p$ and varying values of the parameter $\lambda$ in the presence of a magnetic field ($h = 40$ K). Three phases are recovered as in figure 2. The triangles illustrate positions of TCP at critical values $\gamma^{TCP}$ which are obtained for any values of the parameter $\lambda$ (see text). Full-lines are associated to critical temperatures $T_C$; dashed-lines to positions of first-order transition temperatures $T_{fo}$ and dashed-dotted lines represent the equilibrium temperature $T_{eq}$. Other values of model parameters are: $q = 1$ and $\alpha = 0.5$.

phase boundaries and diagrams are constructed in ($\gamma$, $T_C$) and ($h$, $T_C$) planes (see figures 5–8). In these figures, full lines are second-order phase transition lines ($T_C$) obtained when the global lattice magnetization vanishes continuously and a maximum appears in the response function. At the first-order transition temperatures ($T_{fo}$) which are depicted here by dashed lines, both $m$ and $n_{HS}$ show discontinuities in their behaviors accompanied by discontinuities in the corresponding magnetic susceptibility $\chi$. Dashed-dotted lines are spin-transition lines ($T_{eq}$) which is obtained when the concentration of HS states is $n_{HS} = 0.5$. The triangle points are tricritical points (TCPs) and dotted-lines in figures 6 and 8 are tricritical lines. Figures 5–7 are depicted in ($\gamma$, $T_C$) plane for varying values of parameter $\lambda$ and fixed values of other parameters. Some interesting features emerge from these figures. The spin-transition temperature is constant in a wide range of $\gamma$ for very small values of the parameter $\lambda$. This domain shrinks when $\lambda$ increases. A $\gamma$ range where the tricritical temperature is constant also emerges. A deep analysis of these figures shows that the spin-transition ($T_{eq}$) and the second-order transition ($T_C$) lines meet at the TCP which corresponds to the onset of first-order transitions. It is worthwhile to note that the temperature corresponding to the TCP becomes constant when at least 50% of *nn* bonds are influenced by the exchange interaction $J$. Whenever TCP exists, its position differs slightly from the one found by means of other methods like the CEFT [44], the BL approach [49] and the DMFT approach [48]. These methods and the MFT yield similar finite temperature phase diagrams. But, for the MFT with REI and RMF, at relatively low values of $\gamma$ ($\gamma < \gamma^{TCP}$), two transition temperatures may

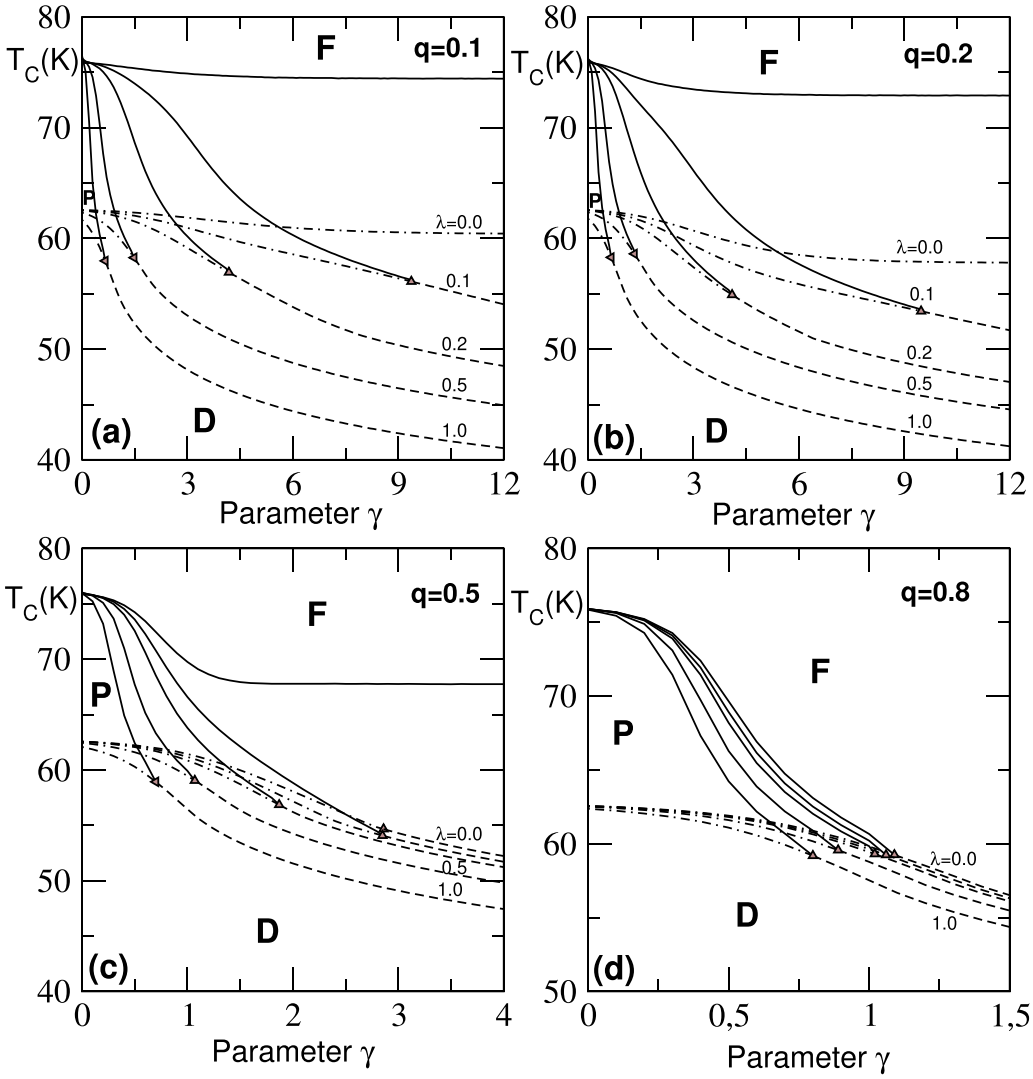


**Figure 7.** Thermal phase diagrams of the system in ($\gamma$, $T_C$) plane for selected values of probability $q$ and varying values of the parameter $\lambda$ with $h = 40$ K and $p = 0.5$. Three phases are found as in two previous figures as well as TCPs. See figure 3 for the nature of each transition line. The TCP does not exist when $q \leqslant 0.5$ (see panels (a)–(c)). Other value of model parameters is $\alpha = 0.5$.

exist: $T_{eq}$ and $T_C$ with $T_{eq} < T_C$. For this range of $\gamma$ values, dia-para and para-ferro magnetic phase transitions are possible and the HS fraction $n_{HS}$ reaches it saturated value ($n_{HS} \simeq 1$). Beyond $\gamma^{TCP}$, the transition is first-order ($T_{fo}$) and only the dia-ferro magnetic phase transition is possible. There, the HS units created interact magnetically and both $m$ and $n_{HS}$ reach their saturated value 1. Note also that for raising values of $\lambda$, $\gamma^{TCP}$ tends to zero. These results bear some resemblance with those reported in [48] (and references therein) using the DMFT approach where increasing values of $\alpha$, $\gamma^{TCP}$ also tends to zero. In zero magnetic field ($h = 0$ K) and for different values of $q$ and $\lambda$, the second-order transition lines ($T_C$) and the spin-transition lines ($T_{eq}$) are almost parallel (see figure 5) in the very low values of $\gamma$ range. But, for higher values of $\gamma$, the transition temperature decreases with $\lambda$ and the model exhibits the tricritical behavior. For $\lambda = 0$, the TCP does not exist when $q \leqslant 0.5$ (figures 5(a)–(c)). For any values of parameter $\gamma$, dia–para and para–ferro magnetic transitions are revealed. These results are also obtained in figure 7 where the magnetic field set to the value $h = 40$ K was randomly distributed in the system with probability $p = 0.5$. Figure 6 shows the influence of the probability $p$ of the distribution of magnetic field $h$ in the system. One observes that for any values of parameter $\lambda$, TCP exist, generating a tricritical line. The study of the effect of the RMF on the system allowed us to plot the phase diagram in ($h$, $T_C$) plane by varying values of the ligand-field strength $\Delta$ and the probability $p$ (figure 8). As we observed previously, three phases are found: dia- (D) para- (P) and ferromagnetic (F) phases. The transition temperature decreases with increasing values of the magnetic field $h$ and increases with the strength of the ligand-field $\Delta$ [44, 48, 49]. For increasing $p$, one shows that the model exhibits the tricritical behavior when $p$ is

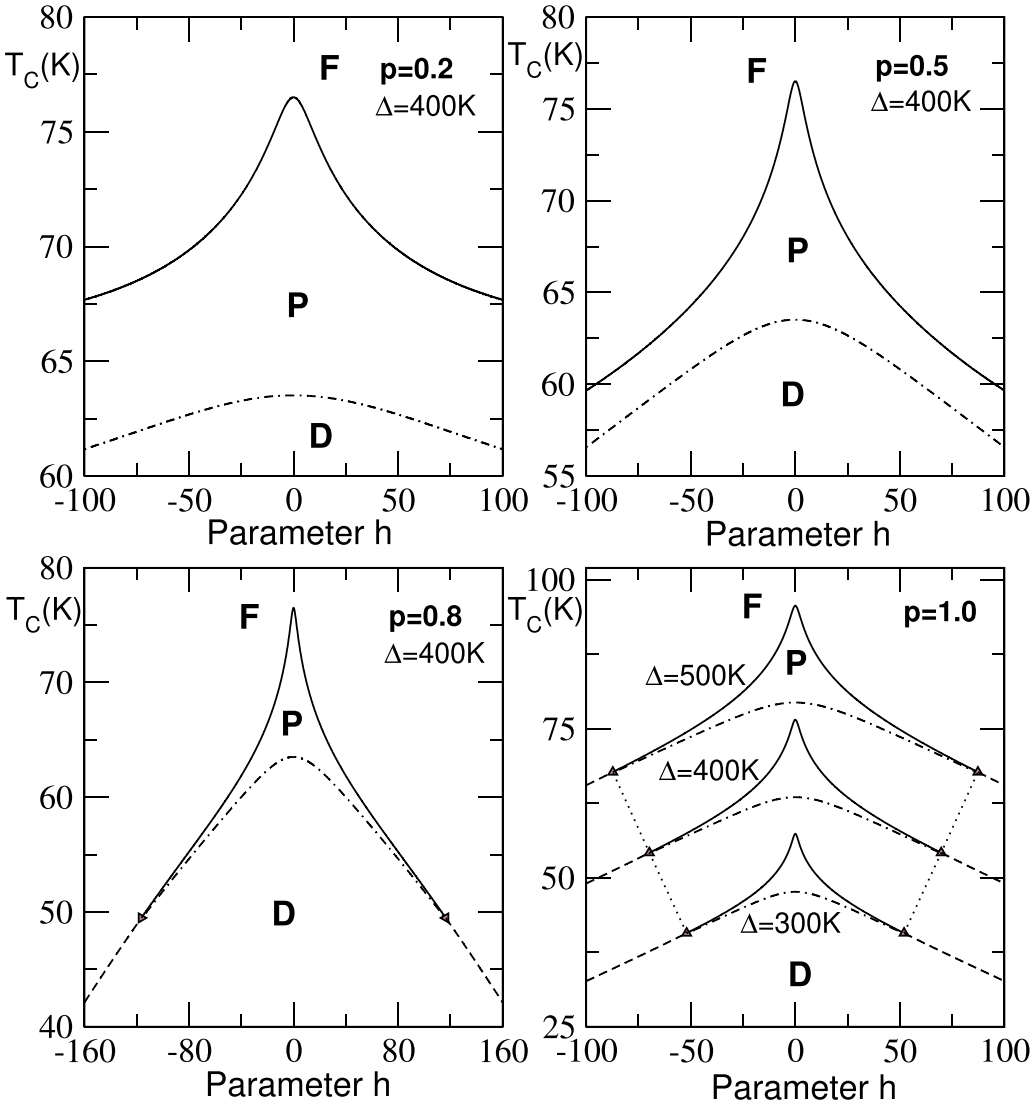


**Figure 8.** Thermal phase diagrams of the model in ($h$, $T_C$) plane for selected values of the probability $p$ and varying values of the ligand-field strength $\Delta$. Three phases as well as TCPs are found as in the three previous figures. The meaning of each transition line is the same as in previous phase diagrams. Other values of system parameters are $q = 1$, $\alpha = 0.5$, $\gamma = 0.5$ and $\lambda = 0$.

relatively high ($p \geqslant 0.8$). In this range of $p$, the TCPs are obtained at $\pm h^{\mathrm{TCP}}$ which tend to zero when $\Delta$ decreases (see figures 8(c) and (d)).

*3.1.2. Hysteretic first-order transition on the magnetization and HS fraction.* In the following, we set values of $p$ and $q$ to 1 and $\lambda = 0$. In this case, the system is subjected to an intense external magnetic field which acts over all SCO sites. At the vicinity of the corresponding first-order transition we perform calculations of the order parameters as function of the applied field strength. This allowed us to display in figures 9 and 10, the resulting magnetic hysteresis loops for some selected values of other model parameters. For these results, the Newton–Raphson method is used to solve equations (12) and (13). It emerges that the system presents three different states: stable states (S) which correspond to the minimal free energy (red parts), unstable states (U) that are associated to the maximum free energy (black parts) and finally metastable states (M) which are intermediate free energy states (blue parts). In figure 9, the hysteresis phenomenon is presented for the magnetization $m$ (left panels) and HS fraction $n_{\mathrm{HS}}$ (right panels) when the temperature is increased. It can be clearly seen that the magnetization loop pattern starts with a small double symmetric loop and as the temperature increases, the deformation disappears leading to a single central loop. The same phenomenon occurs by increasing parameter $\alpha$ or $\gamma$. The opposite phenomenon is observed by raising the ligand-field strength $\Delta$ (see figure 10). With the numerical fixed-point resolution method of equations (12) and (13), one should not observe unstable parts of the hysteresis but instead jumps should occur

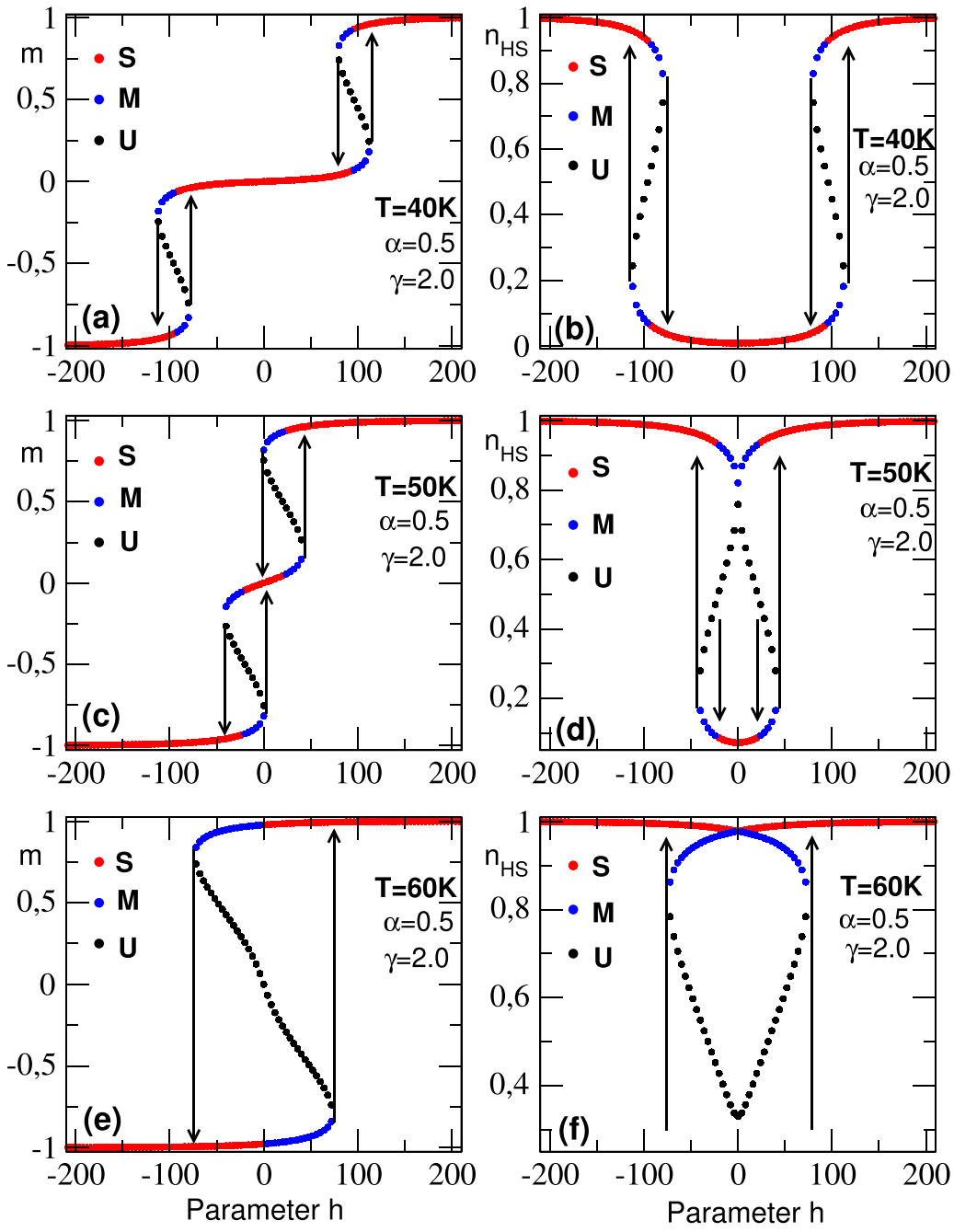


**Figure 9.** Thermally-induced hysteresis loops for the magnetization, $m$, and the HS fraction, $n_{\mathrm{HS}}$, at the vicinity of a first-order transitions. Red, black and blue parts of the hysteresis curves correspond to stable (S), unstable (U) and metastable (M) states of the system respectively. The loop pattern starts with a small double symmetric loop and with increasing temperature, the deformation disappears leading to a single central loop. Values of used parameters are: $p = 1$, $q = 1$, $\lambda = 0$, $\alpha = 0.5$ and $\gamma = 2$.

at the end of metastable states. It appears that the double symmetric loop is obtained when for $h = 0\,\mathrm{K}$, the diamagnetic phase prevails in the system. On the contrary, a single loop appears when the system lays in the ferromagnetic phase. We also study the behavior of the coercive field $h_{\mathrm{C}}$ as a function of parameters $\alpha$ and $\Delta$ for increasing values of the absolute temperature T. As it could be observed in figure 11, $h_{\mathrm{C}+}$ and $h_{\mathrm{C}-}$ associated to positive and negative fields are symmetric with respect to the zero-temperature axis and remain constant in the low-temperature range where the double symmetric loop

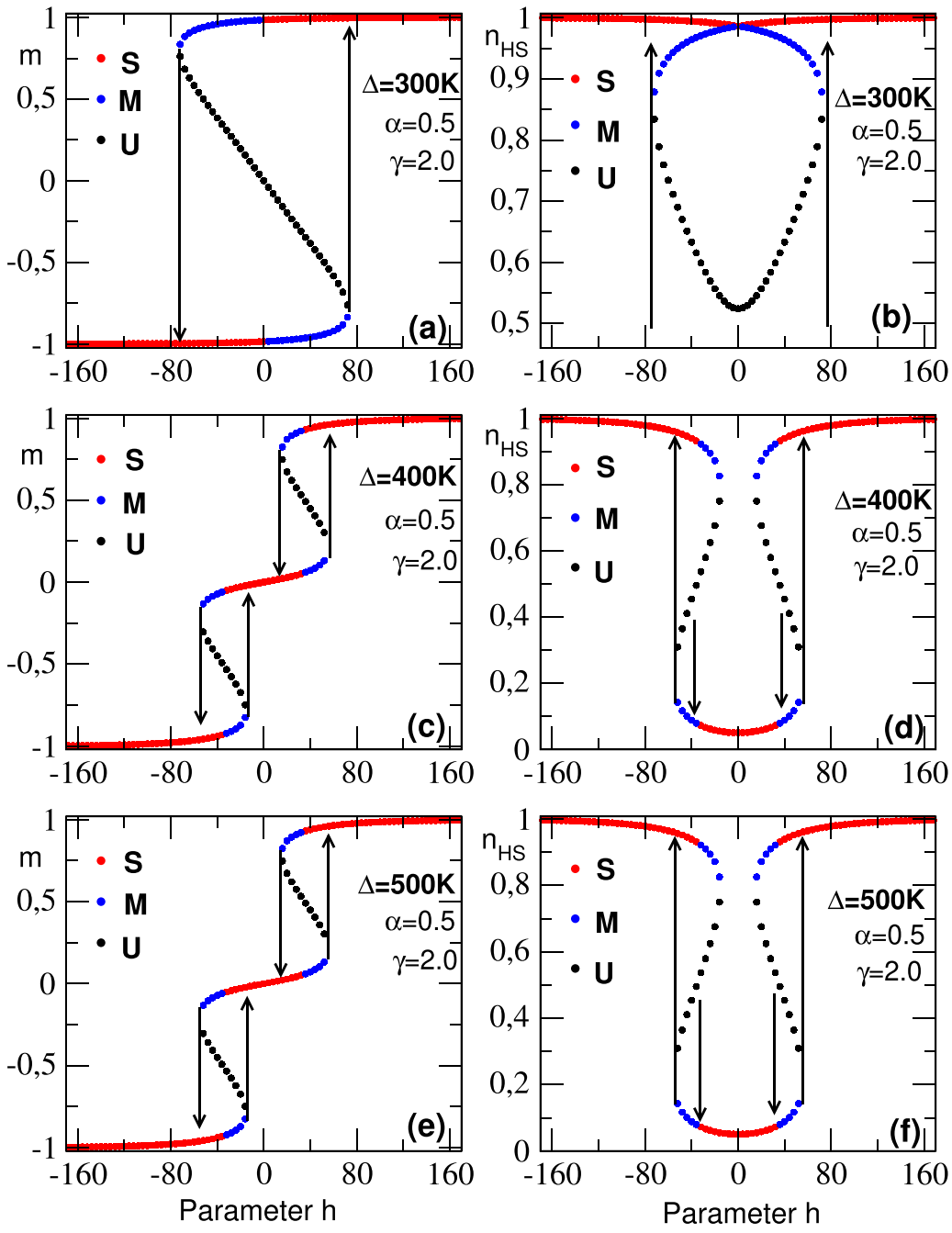


**Figure 10.** Magnetic hysteresis loops for the magnetization $m$ (left panels) and the HS fraction $n_{\mathrm{HS}}$ (right panels) at the vicinity of first-order transitions for some values of the ligand-field strength $\Delta$. Red, black and blue parts of the hysteresis curves correspond to stable (S), unstable (U) and metastable (M) states of the system respectively. Here, the loop pattern starts with a single central loop and becomes a small double symmetric loop when values of $\Delta$ increase. Other values of used parameters are: $p = 1$, $q = 1$, $\lambda = 0$, $\alpha = 0.5$, $\gamma = 2$ and $T = 48$ K.

is observed. When the single central loop is obtained, $h_{\mathrm{C}+}$ increases with temperature whereas $h_{\mathrm{C}-}$ decreases. At fixed temperature, the same phenomenon appears with increasing parameter $\alpha$ whereas the opposite is observed by increasing the ligand-field strength $\Delta$. These results are in good agreement with those reported in figures 9 and 10.

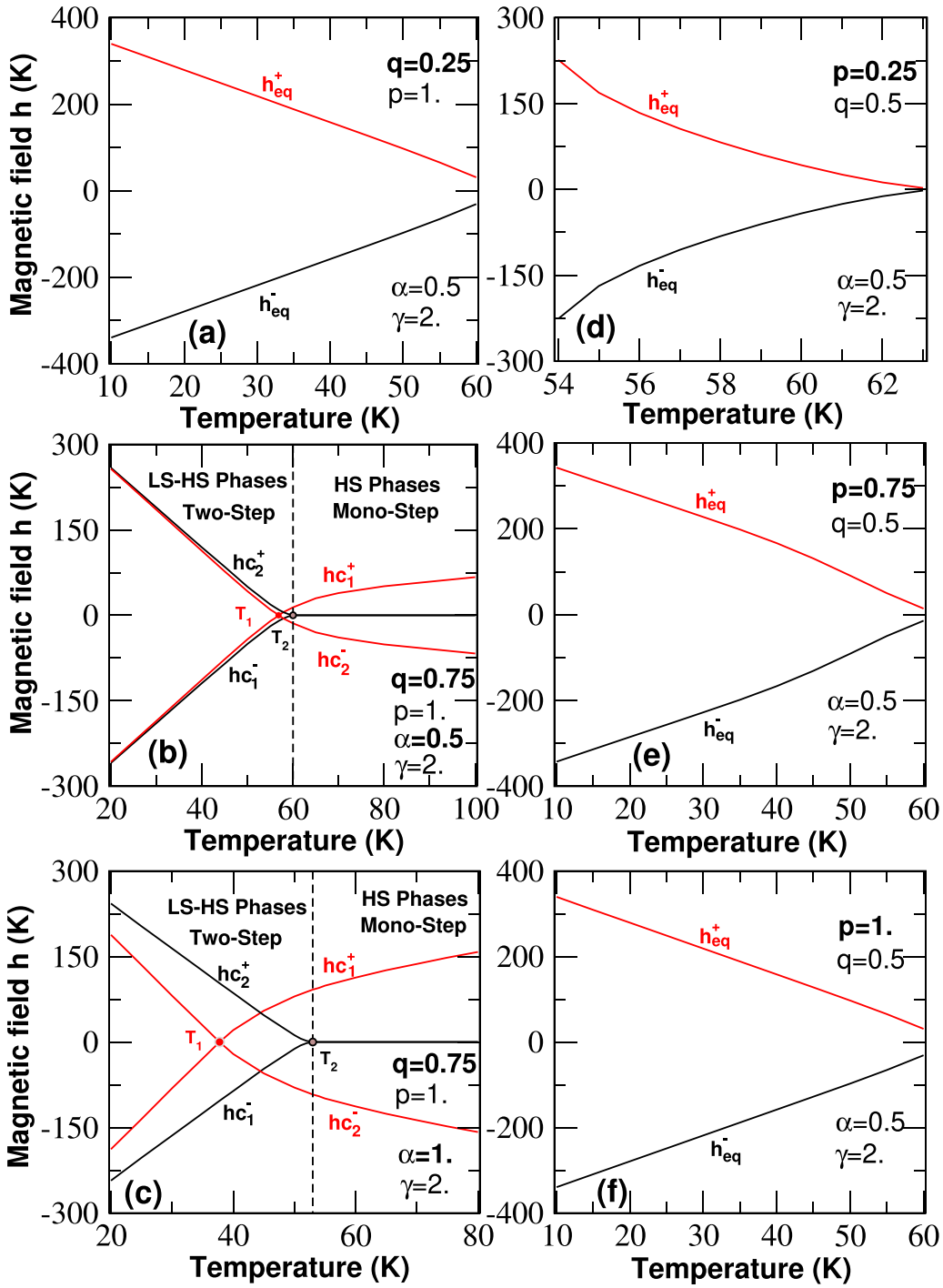


**Figure 11.** Temperature-dependence of the coercive field for selected values of the parameters *p(q),* $\alpha$ and ligand-field strength $\Delta$. $h_{C+}$ corresponds to the coercive field of the upward branch and $h_{C-}$ is associated to that of backward branch. Note that $h_{C+}$ and $h_{C-}$ are symmetric with respect to the zero coercive field axis, being constant at low temperatures, they then evolve in opposite directions as the temperature increases. Other values of used parameters are: $\lambda = 0$ and $\gamma = 2$.

## 4. Conclusion

Using the MFT, we have investigated the magnetic properties of SCO solids that we mapped onto a spin-1 BEG model with exchange interactions $J$ and magnetic field $h$, randomly distributed over the SCO molecules. The main goal of this study was to investigate within MFT, the effects of these random interactions on the system. The iterative method is adopted for the calculation of the order parameters and the corresponding temperature phase diagrams. As in some previous works, the system displays gradual and first-order transitions with varying values of model parameters. Furthermore, TCPs

are obtained when at least 50% of links are under the influence of the exchange interaction. Hence, the exchange interaction plays a crucial role for obtaining the first-order transitions which become sharper and sharper when the system is under the constraint of magnetic field $h$. At the vicinity of first-order transitions, magnetic hysteresis loops are got, and the corresponding coercive field is calculated for varying values of the absolute temperature. The existence of the hysteresis phenomenon is much used to enhance the performance of SCO solids in technology.

## Data availability statement

The data that support the findings of this study are available from the corresponding author [T D Oke] upon reasonable request.

## Acknowledgments

This research was funded by the IMSP and the University of Abomey-Calavi, Agence Nationale de la Recherche Scientifique, Grant Number Mol-CoSM No. ANR-20-CE07-0028-02, the Universities of Versailles and Paris-Saclay-UPSAY, and the Centre National de la Recherche Scientifique through the MITI interdisciplinary Programs through its exploratory research Program.

## Authors contributions

All authors equally contribute to the present work in the calculations and in the manuscript writing process.

## Conflicts of interest

The authors declare no competing financial interest.

## Ethics statement

The results that report in this work not involve research practices on humans and animals.

## ORCID iDs

Toussaint Djidjoho Oke https://orcid.org/0000-0001-7069-6224
Kamel Boukheddaden https://orcid.org/0000-0003-0464-1609

## References

[1] Gütlich P 1981 *Struct. Bond.* **44** 83
[2] König E 1991 *Struct. Bond.* **76** 51
[3] Kahn O 1996 *Curr. Opin. Solid State Mater. Sci.* **1** 547
[4] Cambi L and Gagnasso A 1931 *Atti Accad. Naz. Lencei.* **13** 809
[5] Chiruta D, Jureschi C M, Linares J, Garcia Y and Rotaru A 2014 *J. Appl. Phys.* **115** 053523
[6] Gütluch P and Goodwin H A 2004 *Spin-Crossover in Transition Metal Compounds I, II, III* (Springer) pp 233–5
[7] Bousseksou A, Molnár G, Salmon L and Nicolazzi W 2011 *Chem. Soc. Rev.* **40** 3313
[8] Linares J, Codjovi E and Garcia Y 2012 *Sensor* **12** 4479
[9] Dîrtu M M, Schmit F, Naik A D, Rotaru A, Marchand-Brynaert J and Garcia Y 2011 *Int. J. Mol. Sci.* **12** 5339
[10] Gütlich P, Gasper A B and Garcia Y 2013 *Beilstein J. Org. Chem.* **9** 342
[11] Rotaru A, Gural'Skiy I A, Molnár G, Salmon L, Demont P and Bousseksou A 2012 *Chem. Commun.* **48** 4163
[12] Rotaru A, Dugay J, Tan R P, Gural'skiy I A, Salmon L, Demont P, Carrey J, Molnár G, Respaud M and Bousseksou A 2013 *Adv. Mater.* **25** 1745
[13] Tokoro H, Ohkoshi S I and Hashimoto K 2003 *Appl. Phys. Lett.* **82** 1245
[14] Varret F, Boukheddaden K, Chong C, Goujon A, Gillon B, Jeftic J and Hauser A 2007 *Eur. Phys. Lett.* **77** 30007
[15] Pejaković D A, Manson J L, Kitamura C, Miller J S and Epstein A J 2001 *Polyhedron* **20** 1435
[16] Kato K, Moritono Y, Takata M, Sakata M, Umekawa M, Hamada N, Ohkoshi S, Tokoro H and Hashimoto K 2003 *Phys. Rev. Lett.* **91** 255502
[17] Nasser J A, Topçu S, Chassagne L, Wakim M, Bennali B, Linares J and Alayli Y 2011 *Eur. Phys. J.* B **83** 115
[18] Gütlich P, Garcia Y and Goodwin H A 2000 *Chem. Soc. Rev.* **29** 419
[19] Rao C N R 1985 *Int. Rev. Phys. Chem.* **4** 19
[20] König E, Ritter G and Kulshreshtha S K 1985 *Chem. Rev.* **85** 219
[21] Benerjee H, Chakraborty S and Saha-Dasgupta T 2017 *Inorganics* **5** 47
[22] Gîndulescu A, Rotaru A, Linares J, Dimian M and Nasser J 2011 *J. Phys: Conf. Ser.* **268** 012007
[23] Nishino M, Miyashita S and Rikvold P A 2017 *Phys. Rev.* B **96** 144425
[24] Enachescu C, Stoleriu L, Stancu A and Hauser A 2010 *Phys. Rev.* B **82** 104114
[25] Sorai M and Seki S 1974 *J. Phys. Chem. Solids* **35** 555
[26] Paez-Espejo M, Sy M and Boukheddaden K 2016 *J. Am. Chem. Soc.* **138** 3202
[27] Halcrow M A 2013 *Spin-Crossover Materials: Properties and Applications* (Wiley)
[28] Quintero C M, Félix G, Souleimanov I, Costa J S, Molnár G, Salmon L, Nicolazzi W and Bousseksou A 2014 *Beilstein J. Nanotechnol.* **5** 2230
[29] Spiering H and Willenbacher N 1989 *J. Phys.: Condens. Matter* **1** 10089
[30] Gudyma I, Ivashko V and Linares J 2014 *J. Appl. Phys.* **116** 173509
[31] Nishino M, Miyashita S and Boukheddaden K 2003 *J. Chem. Phys.* **118** 4594
[32] Wajnflasz J 1970 *Phys. Status Solidi* B **40** 537
[33] Nasser J A 2001 *Eur. Phys. J.* B **21** 3–10 Nasser J A 2005 *Eur. Phys. J.* B **48** 19–27 and references therein
[34] Rotaru A, Carmona A, Combaud F, Linares J, Stancu A and Nasser J 2009 *Polyhedron* **28** 1684
[35] Rotaru A, Linares J, Mordelet S, Stancu A and Nasser J 2009 *J. Appl. Phys.* **106** 043507
[36] Rotaru A, Linares J, Codjovi E, Nasser J and Stancu A 2008 *J. Appl. Phys.* **103** 07B908
[37] Enachescu C, Stoleriu L, Stancu A and Hauser A 2009 *Phys. Rev. Lett.* **102** 257204
[38] Nishino M, Boukheddaden K and Miyashita S 2009 *Phys. Rev.* B **79** 012409

[39] Slimani A, Boukheddaden K and Yamashita K 2015 *Phys. Rev.* B **92** 014111
[40] Nishino M and Miyashita S 2013 *Phys. Rev.* B **88** 014108
[41] Boukheddaden K, Nishino M and Miyashita S 2007 *Phys. Rev.* B **75** 094112
[42] Nasser J A, Boukheddaden K and Linares J 2004 *Eur. Phys. J.* B **39** 219
[43] Boukheddaden K, Miyashita S and Nishino M 2008 *Phys. Rev. Lett.* **100** 177206
[44] Oke T D, Hontinfinde F and Boukheddaden K 2013 *Eur. Phys. J.* B **86** 271
[45] Ogou S B, Oke T D, Hontinfinde F and Boukheddaden K 2019 *Adv. Theory Simul.* **2** 1800192
[46] Oke T D, Ndiaye M, Hontinfinde F and Boukheddaden K 2021 *Eur. Phys. J.* B **94** 38
[47] Oke T D, Ogou S B, Hontinfinde F and Boukheddaden K 2022 *Eur. Phys. J.* B **95** 96
[48] Oke T D, Hontinfinde F and Boukheddaden K 2015 *Appl. Phys.* A **120** 309
[49] Oke T D, Hontinfinde F and Boukheddaden K 2016 *Comput. Condens. Matter.* **9** 27
[50] Albayrak E 2018 *Chin. J. Phys.* **56** 622
[51] Karimou M, Albayrak E, Tessilimy A, Hontinfinde F and Yessoufou R 2017 *Chin. J. Phys.* **55** 2371
[52] Bahmad L, Benyousself A and El Kenz A 2008 *Physica* A **387** 825
[53] Albayrak E and Karimou M 2017 *Chin. J. Phys.* **55** 1361
[54] Albayrak E and Karimou M 2018 *Int. J. Theor. Phys.* **57** 715
[55] Ribeiro P O, Alho B P, Ribas R M, Nóbrega E P, de Sousa V S R, von Ranke P J 2019 *J. Magn. Magn. Mater.* **489** 165340
[56] Boukheddaden K, Nishino M, Miyashita S and Varret F 2005 *Phys. Rev.* B **72** 014467
[57] Gudyma I, Boboshko K and Boukheddaden K 2020 *Phys. Lett.* A **384** 126677
[58] Gudyma I and Yarema V 2022 *Appl. Nanosci.* **12** 747 Gudyma I, Yarema V *Appl. Nanosci.* (https://doi.org/10.1007/s13204-022-02739-5)
[59] Slimani A, Boukheddaden K, Varret F, Oubouchou H, Nishino M and Miyashita S 2013 *Phys. Rev.* B **87** 014111
[60] Zhang Y 2020 *J. Chem. Phys.* **153** 134704